Cell

Insight into Structure and Assembly of the Nuclear Pore Complex by Utilizing the Genome of a Eukaryotic Thermophile

Stefan Amlacher,[1,3] Phillip Sarges,[1,3] Dirk Flemming,[1,3] Vera van Noort,[2,3] Ruth Kunze,[1] Damien P. Devos,[2] Manimozhiyan Arumugam,[2] Peer Bork,[2,*] and Ed Hurt[1,*]
[1]Biochemie-Zentrum der Universität Heidelberg, Im Neuenheimer Feld 328, Heidelberg D-69120, Germany
[2]EMBL, Meyerhofstrasse 1, Heidelberg D-69117, Germany
[3]These authors contributed equally to this work
*Correspondence: bork@embl.de (P.B.), ed.hurt@bzh.uni-heidelberg.de (E.H.)
DOI 10.1016/j.cell.2011.06.039

SUMMARY

Despite decades of research, the structure and assembly of the nuclear pore complex (NPC), which is composed of ~30 nucleoporins (Nups), remain elusive. Here, we report the genome of the thermophilic fungus *Chaetomium thermophilum* (*ct*) and identify the complete repertoire of Nups therein. The thermophilic proteins show improved properties for structural and biochemical studies compared to their mesophilic counterparts, and purified *ct*Nups enabled the reconstitution of the inner pore ring module that spans the width of the NPC from the anchoring membrane to the central transport channel. This module is composed of two large Nups, Nup192 and Nup170, which are flexibly bridged by short linear motifs made up of linker Nups, Nic96 and Nup53. This assembly illustrates how Nup interactions can generate structural plasticity within the NPC scaffold. Our findings therefore demonstrate the utility of the genome of a thermophilic eukaryote for studying complex molecular machines.

INTRODUCTION

The conserved nuclear pore complexes (NPCs) spanning the double nuclear membrane are the sole mediators of transport between the nucleus and the cytoplasm. The NPC is an ~50 MDa structure displaying an eight-fold symmetry and consisting of a number of distinct substructures: the spoke-ring complex, the cytoplasmic pore filaments, the nuclear basket, and the central channel, through which nucleocytoplasmic transport occurs (Fahrenkrog and Aebi, 2003). The NPC consists of ~30 different proteins named nucleoporins, or Nups, that were initially identified by nuclear fractionation, with the help of antibodies or lectins, through genetic screens, and by affinity purification (for review, see Doye and Hurt, 1997). Subsequently, complete NPCs were isolated revealing the entire set of Nups for both yeast and vertebrates (Cronshaw et al., 2002; Rout et al., 2000). Each Nup is present in multiple copies (8, 16, or 32) with a total of ~500 Nups per NPC (Alber et al., 2007). One group of Nups contains phenylalanine-glycine (FG)-rich repeat domains that line the central transport channel, allowing shuttling transport receptors to pass through a mesh of FG nucleoporins via transient interactions with these FG motifs (Patel et al., 2007). The other group of Nups, which is devoid of FG repeats, constitutes the NPC core structure.

The majority of Nups are part of discrete subcomplexes, which are conserved from yeast to humans and are the building blocks of the NPC (D'Angelo and Hetzer, 2008). Biochemically defined NPC subcomplexes in yeast include the following: (1) the Y-shaped Nup84 complex (Siniossoglou et al., 1996), (2) the Nsp1 complex, a module held together by coiled-coil interactions and with FG repeats protruding into the central pore channel (Grandi et al., 1993), (3) the Nup82 complex, which is located at the cytoplasmic face (Belgareh et al., 1998; Hurwitz et al., 1998), (4) the Nup60-Nup2 heterodimer, which is located on the nucleoplasmic side of the NPC (Dilworth et al., 2001), (5) the Nup170-Nup53/Nup59 complex (Marelli et al., 1998), which is essential for NPC assembly (Makio et al., 2009), and (6) the Ndc1 complex, an assembly of three integral membrane proteins inserted in the pore membrane (Onischenko et al., 2009).

The two largest structural Nups from yeast, Nup192 and Nup188, have not been isolated in stable subcomplexes, but substoichiometric interactions have been reported between Nic96 and either Nup188 or Nup192 (Kosova et al., 1999; Nehrbass et al., 1996). Moreover, two-hybrid screens demonstrated an interaction between Nic96 and Nup53 (Fahrenkrog et al., 2000), implying an association between Nic96 and the Nup170 subcomplex.

The large structural Nups are predicted to have either an α-helical structure (Nup192, Nup188) or a combined β-propeller/α-solenoid fold (Nup170, Nup157) (Devos et al., 2006). However, it remains unknown whether they directly interact with each other and how they are linked to the other NPC modules. Current models predict a cage-like or fence-like NPC scaffold formed by Nups with β-propeller and/or α-solenoid folds, such as the Y-shaped Nup84 complex (Brohawn et al., 2008; Devos et al., 2004; Hsia et al., 2007). Despite these insights into NPC structure

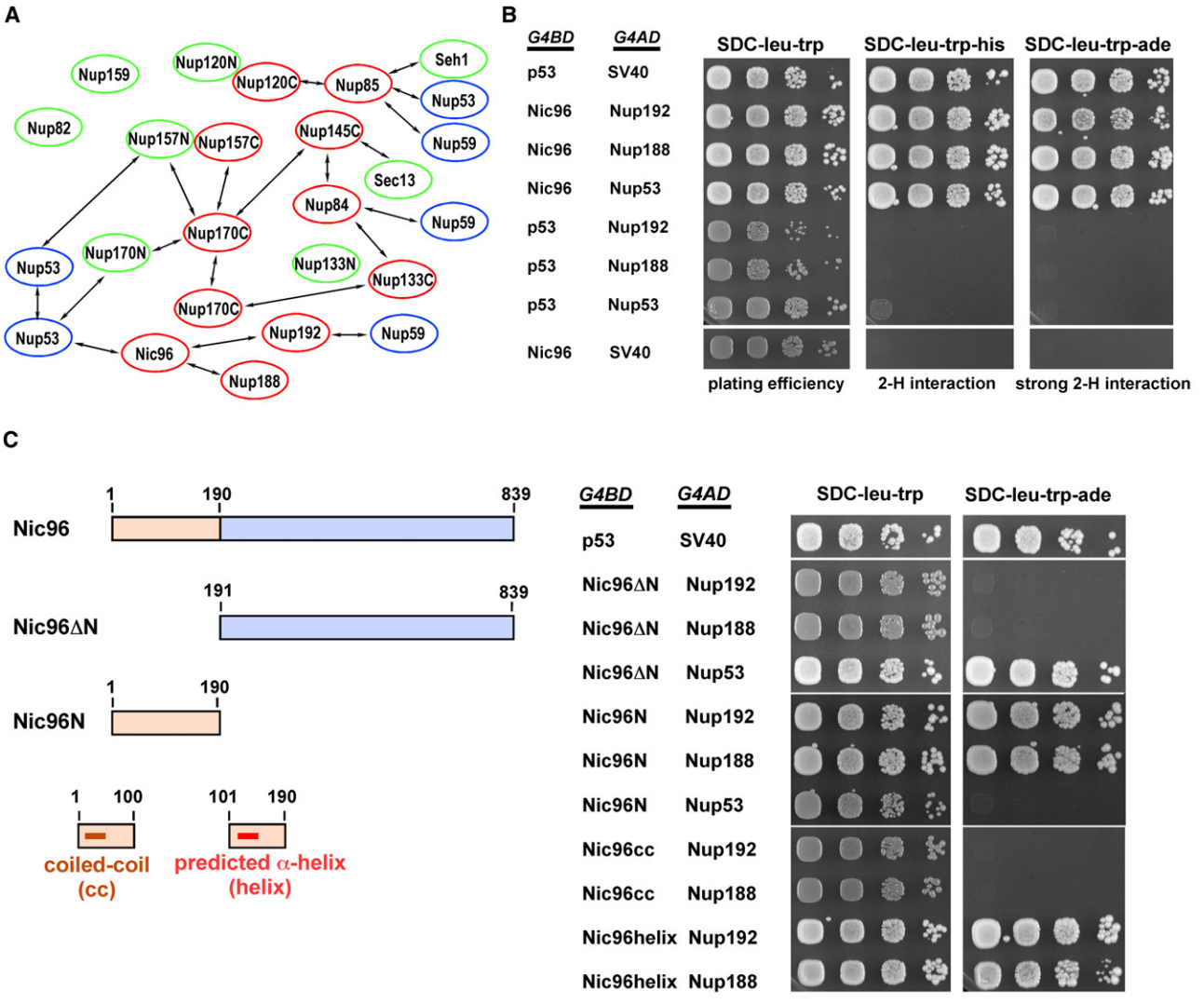
A
Nup159
Nup120N
Nup120C
Nup85
Seh1
Nup53
Nup59
Nup82
Nup157N
Nup157C
Nup145C
Sec13
Nup84
Nup59
Nup170C
Nup170N
Nup53
Nup133N
Nup133C
Nup170C
Nup53
Nup192
Nup59
Nic96
Nup188
B
G4BD
G4AD
p53 SV40
Nic96 Nup192
Nic96 Nup188
Nic96 Nup53
p53 Nup192
p53 Nup188
p53 Nup53
Nic96 SV40
SDC-leu-trp
SDC-leu-trp-his
SDC-leu-trp-ade
plating efficiency
2-H interaction
strong 2-H interaction
C
Nic96
1
190
839
Nic96ΔN
191
839
Nic96N
1
190
1
100
101
190
coiled-coil (cc)
predicted α-helix (helix)
G4BD
G4AD
p53 SV40
Nic96ΔN Nup192
Nic96ΔN Nup188
Nic96ΔN Nup53
Nic96N Nup192
Nic96N Nup188
Nic96N Nup53
Nic96cc Nup192
Nic96cc Nup188
Nic96helix Nup192
Nic96helix Nup188
SDC-leu-trp
SDC-leu-trp-ade
D
coiled-coil
predicted α-helix
crystal structure
S.c.
P.s.
C.t.
C.g.
N.c.
H.s.
X.l.
D.m.

and assembly, key questions remain. Central to this is how the building blocks of the NPC, the ~30 Nups and their derived subcomplexes, make up the major substructures of the NPC scaffold. In particular, the formation of the inner pore ring (also called spoke ring or equatorial ring) by the large Nups, Nup192, Nup188, Nup170, and Nup157, remained elusive.

In this study, we report the genome of a thermophilic eukaryote, which was found to be well suited for biochemical studies of Nups. The Nups identified in the fungus *Chaetomium thermophilum* enabled reconstitution of the NPC module that forms the inner pore ring. This assembly, which potentially spans from the pore membrane to the FG transport channel, consists of Nup192 and Nup170, bridged by Nic96 and Nup53. Within this complex, we have identified nucleoporin interactions that depend on short and flexible motifs. Electron microscopy demonstrates that Nup192 and Nup188 exhibit an ''S''-like morphology that resembles the shapes of karyopherins, which are shuttling nuclear transport receptors. Collectively, our findings support the hypothesis that the large structural Nups preferentially bind short linear motifs provided by linker Nups for assembly into the NPC scaffold.

RESULTS

Two-Hybrid Analysis Identifies New Nup Interactions

To identify the connectivity and physical interactions between the structural Nups in the NPC framework, we performed a two-hybrid analysis with yeast Nups. We focused on Nups predicted to form α-helical, β-propeller, or a combination of the two folds because these predominant fold-types in the NPC are thought to significantly contribute to multiple Nup interactions. These investigations not only recapitulated some of the known Nup associations but also revealed unidentified interactions including that of Nic96 with either Nup192 or Nup188 (Figures 1A and 1B). Shortening of the interacting motif in Nic96 identified a relatively short sequence in the N domain (residues 101–190) that was necessary and sufficient to bind to full-length Nup192 or Nup188 (Figure 1C), or derived C domains ($Nup192_{553–1683}$ and $Nup188_{561–1655}$), but not smaller constructs (data not shown). Sequence analysis indicated that the binding motif in Nic96 contains a predicted α helix of ~60 amino acids (residues 109–164) that is conserved with a characteristic spacing of hydrophobic residues and interspersed charged amino acids (Figures 1C and 1D). In contrast, the conserved coiled-coil domain in the N-terminal part of Nic96 (residues 1–100) that was previously shown to recruit the Nsp1-Nup49-Nup57 core complex (Grandi et al., 1993) did not interact with Nup192 or Nup188 in the two-hybrid assay (Figure 1C). Thus, a previously unknown motif in the flexible N-terminal domain of Nic96 interacts with Nup192 and Nup188.

We performed genetic analyses to demonstrate a requirement of the Nic96 helix motif for NPC structure and assembly. Deletion of a sequence from Nic96 containing the helix motif (*nic96Δ101–190*) caused a mild growth defect at 23°C, whereas deletion of the coiled-coil domain (*nic96Δ1–100*) retarded cell growth more significantly (Figure S1A available online). However, when both the coiled-coil and the adjacent helix motifs were deleted (*nic96Δ1–190*), an extremely slow growth phenotype was generated. Thus, the synergistic intramolecular overlap between these two motifs suggests that recruitment of the Nsp1 core complex via the coiled-coil sequence and binding of Nup192 or Nup188 via the adjacent helix are essential for Nic96 function.

A functional overlap of the Nic96 helix with Nup192 or Nup188 was investigated by genetic analysis. Combination of viable *nup192* mutants with the *nic96Δhelix* allele resulted in synthetic lethality (Figure S1B). In contrast, the *nic96* mutant lacking the coiled-coil sequence was not genetically linked to these *nup192* alleles (Figure S1B and data not shown). Combination of the viable *nup188Δ* mutant with *nic96Δhelix* was not lethal but resulted in a synergistically enhanced growth defect (data not shown) with a failure to efficiently target Nup192-GFP to the NPCs (Figure S1C). These data indicate that Nic96 is functionally linked to Nup192 and Nup188 via its N-terminal helix motif, which facilitates assembly of these large structural Nups into the NPC.

Superior Nucleoporin Properties Enabled by a Thermophilic Eukaryote

Next we sought to verify the two-hybrid interaction found between the large structural Nups and Nic96. In order to do this, we purified Nup192, Nup188, and Nic96, either directly from yeast or recombinantly from *E. coli*, and performed in vitro reconstitution studies. However, these studies were not conclusive due to both a modest yield and stability of the large structural Nups (data not shown). In order to improve the outcome of these studies, we performed reconstitution studies with Nups derived from a thermophilic eukaryote. It was assumed that these Nups could display improved biochemical and structural properties after isolation, as observed for thermostable proteins from thermophilic prokaryotes.

Among eukaryotes, only a few microorganisms have the capability to grow at temperatures above 50°C (Hickey and Singer, 2004). One of them is the fungus *C. thermophilum*, which can thrive at temperatures of up to 60°C (La Touche, 1948). This thermophilic, filamentous ascomycete is a member of the family *Chaetomiaceae*, which is found in soil, dung, or rotting plants.

Figure 1. Two-Hybrid Screen Identifies New Interactions between Yeast Nucleoporins

(A) Two-hybrid interactions between yeast Nups (indicated by black arrows). Nups with predicted α-helical (red) or β-propeller (green) folds. Nup53/Nup59 (blue).

(B) Two-hybrid interaction between Nic96 and Nup188 or Nup192, and between Nup53 and Nic96. Two-hybrid plasmids expressing the indicated *G4BD* (*GAL4* DNA-binding domain) and *G4AD* (*GAL4* activation domain) constructs were transformed into a yeast reporter strain and grown on the indicated plates.

(C) Nup188 and Nup192 interact with a predicted α helix in the Nic96 N domain. Two-hybrid interactions between the indicated Nic96 constructs and Nup188/Nup192 (right panel).

(D) Sequence alignment, using ClustalW2 and *Jalview*, of Nic96/Nup93 orthologs from *Saccharomyces cerevisiae* (*S.c.*), *Pichia stipitis* (*P.s.*), *Chaetomium thermophilum* (*C.t.*), *Chaetomium globosum* (*C.g.*), *Neurospora crassa* (*N.c.*), *Homo sapiens* (*H.s.*), *Xenopus laevis* (*X.l.*), and *Drosophila melanogaster* (*D.m.*). See also Figure S1.

It contributes significantly to the breakdown of cellulose with a high-temperature decompostation phase (>55°C), which only allows thermophilic organisms including *C. thermophilum* to grow. This suggests that the proteome of *C. thermophilum* is more stably folded than that of its mesophilic relatives. Indeed, analysis of a few enzymes (e.g., xylanases) cloned from *C. thermophilum* indicated thermostability at up to 60°C (Hakulinen et al., 2003). Remarkably, *C. thermophilum* is most closely related to the mesophilic mold fungus *Chaetomium globosum* (optimal growth temperature of ~24°C), a frequent indoor contaminant generating mycotoxins and encountered as a causative agent of skin and nail infections in humans.

To gain insight into the morphology of *C. thermophilum*, we performed light and electron microscopy of cells grown at 50°C. This analysis revealed that this thermophile is a mycelium-forming fungus with multinucleate hyphae that are perforated by septa as observed for other filamentous ascomycetes such as *Neurospora crassa* or *Aspergillus nidulans* (Figure S2). *C. thermophilum* exhibits a nucleus and a distinct nucleolus surrounded by the double nuclear membrane with interspersed NPCs. Sporadically, a spindle pole body associated with the nuclear membrane or a dividing nucleus can be seen, which points to a closed mitosis (see Discussion). Further conspicuous structures in the thin-sectioned cells are mitochondria with numerous christae, ER membranes, vesicles, and multivesicular bodies proving that *C. thermophilum* is a typical eukaryote with distinct compartments and organellar structures known from mesophilic eukaryotes.

Encouraged by our consideration to have access to thermostable nucleoporins, we sought to sequence the genome of *C. thermophilum.* We used the isolate of *C. thermophilum* derived from fermenting straw by La Touche in 1948, grown at 50°C, to extract DNA (Figure S2A). The genome of *C. thermophilum* was sequenced using the Roche 454 FLX and XLR platforms (Margulies et al., 2005; Ronaghi et al., 1996) and a 24-fold coverage assembly was obtained that separated into 20 scaffolds (only 4 more than expected from the 8 chromosomes), implying a high assembly quality (Table S1). Based on abundance differences of reads, we were also able to separate and completely assemble the mitochondrial genome (127 kb containing 15 protein-coding and 28 tRNA genes) and conclude that per nuclear genome 40 mitochondrial genomes exist. In the nuclear genome of 28.3 Mb, we predicted 243 tRNA genes and found the rRNA operon at ~1500-fold coverage, but currently it cannot be assembled as part of the scaffolds. Based on 21,141 independently sequenced cDNAs sequences, the total coverage of the nuclear genome was estimated to be 96%. Using a set of 4,011 single-copy orthologs, derived for the subphylum of *Pezizomycotina*, the gene coverage was in close agreement to this figure at 98.6%. In total, we identified 7,227 protein-coding genes (Table S1) by ab initio gene prediction with AUGUSTUS (Stanke and Waack, 2003), of which 6,862 could be mapped to orthologous groups using the eggNOG pipeline (Muller et al., 2010). The genome and proteome sequence of *C. thermophilum* is available at NCBI GenBank or at http://ct.bork.embl.de, where it can be subjected to various queries, e.g., for the *C. thermophilum* genes (by name, position, or PFAM domains, etc.), or where BLAST can be run with a mesophilic protein of interest against the predicted *C. thermophilum* proteome. For 4,230 (73%) out of 5,797 *S. cerevisiae* proteins, a homolog exists in *C. thermophilum* that can be used for homology modeling. Similarly, there are homologs in *C. thermophilum* for 10,191 (44%) out of 22,937 human proteins including many families that cannot be found in prokaryotes.

Searches in the *C. thermophilum* genome demonstrated that all of the Nups, which are conserved from yeast to humans, are present in this eukaryotic thermophile (Table S2 and Figure S3). As gene order is only conserved within close relatives to *C. thermophilum* (data not shown), synteny could not be used to confirm orthology. Orthology could be confirmed by triangles of reciprocal best BLAST (Altschul et al., 1997) hits as implemented in eggNOG v2 (Muller et al., 2010) for 20 *ct*Nups; the others were confirmed by using the *ct*Nup as query for psiBLAST and retrieving the original Nup. Central to this study, we identified and subsequently analyzed the *C. thermophilum* (*ct*) orthologs of the yeast Nup192 (196.9 kDa), Nup188 (203.7 kDa), Nup170 (156.2 kDa), Nic96 (121.3 kDa), and Nup53 (46.9 kDa). Multiple sequence alignments with derived average distance trees indicate that the *ct*Nups are most closely related to the annotated orthologs of *C. globosum,* followed by *Podospora anserina, N. crassa*, and *A. nidulans*, which are all members of the *Pezizomycotina* clade. Importantly, the *ct*Nups are related, albeit more distantly, to their well-studied mesophilic orthologs from *Saccharomyces cerevisiae*, *Schizosaccharomyces pombe*, and *Homo sapiens* (Figure S4).

The genes encoding these thermophilic Nups were cloned from genomic DNA or, when necessary, from cDNA (see Experimental Procedures) and heterologously expressed in yeast. This approach was specifically chosen because the behavior of the large structural *ct*Nups (>150 kDa) in the eukaryotic expression system was superior to that of *ct*Nup expression in *E. coli* (data not shown). Analysis of affinity-purified thermophilic Nups by SDS-PAGE and Coomassie staining revealed that the large structural Nups, *ct*Nup192, *ct*Nup188, and *ct*Nup170, could be purified in significantly higher amounts than the corresponding yeast orthologs with little degradation or contamination (Figure 2A).

The isolated *ct*Nups exhibited an increased thermosolubility when compared to their yeast counterparts. Strikingly, purified *ct*Nup192 and *ct*Nup170 remained soluble at temperatures of up to 57°C, which is close to the temperature at which this thermophilic fungus ceases growth (Figure 2B). In contrast, purified yeast Nup192 and Nup170 precipitated at 36°C (Figure 2B and data not shown). Moreover, the large structural Nups eluted from the gel filtration column predominantly as monomeric proteins (Figure 2C). Thus, heterologous gene expression in yeast yielded monomeric *ct*Nups that could be purified in high quantities (approximately 3 mg from a 10 l culture) and with increased thermostability.

In Vitro Reconstitution of Nup Interactions with Nups from *C. thermophilum*

Next, we used the purified large Nups from *C. thermophilum* for in vitro reconstitution. Initially, we focused on the interactions

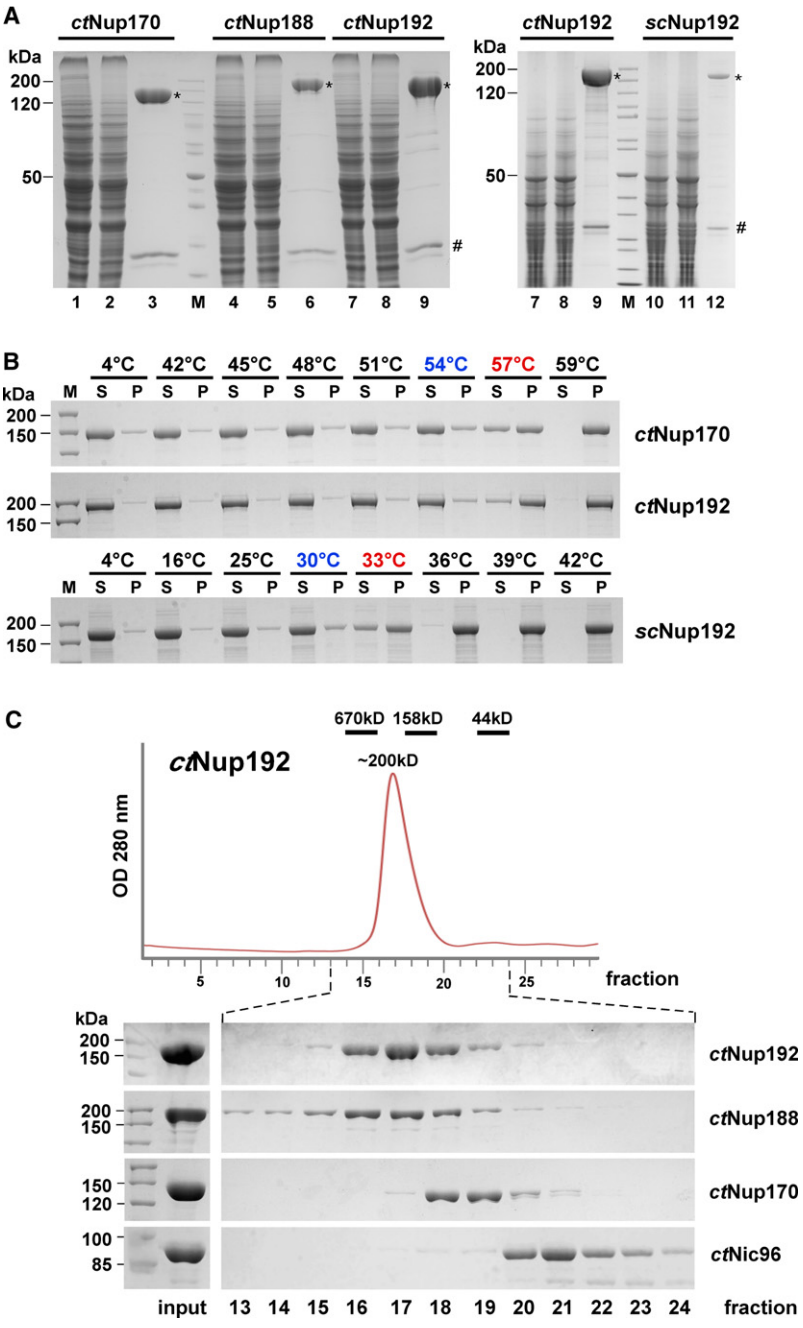

Figure 2. Purification and Stability of *C. thermophilum* Nups

(A) Affinity purification of *ct*Nup170, *ct*Nup188, and *ct*Nup192, in comparison to yeast *sc*Nup192. Lysate (lanes 1, 4, 7, 10), unbound proteins (2, 5, 8,11) and TEV-eluates (3, 6, 9, 12) were analyzed by SDS-PAGE and Coomassie staining. Affinity-purified Nups (*). TEV protease (#). Marker (M).

(B) Thermosolubility (in vitro aggregation) test for yeast and *ct*Nups. Affinity-purified *ct*Nup170, *ct*Nup192, and yeast *sc*Nup192 were incubated at the indicated temperatures for 1 hr, before supernatant (S) and pellet (P) fractions obtained by centrifugation were analyzed by SDS-PAGE and Coomassie staining.

(C) Gel-filtration chromatography of the indicated purified *ct*Nups on Superdex 200. Input and fractions were analyzed by SDS-PAGE and Coomassie staining (lower graph).

See also Figure S2, Figure S3, Figure S4, Table S1, and Table S2.

between Nic96 and Nup192 or Nup188 that were identified in the two-hybrid screen. ProtA-tagged *ct*Nic96 (for sequence see Figure S5A) was affinity-purified on IgG-Sepharose and incubated with purified *ct*Nup192 or *ct*Nup188 in the presence of a competing lysate. As shown by SDS-PAGE and Coomassie staining, *ct*Nic96 requires the conserved amino-terminal helix motif identified in the yeast system to bind to either *ct*Nup192 or *ct*Nup188 (Figure 3A) yielding stoichiometric heterodimers (Figure 3B). Moreover, the purified *ct*Nic96 helix alone was able to mediate binding to *ct*Nup192 or *ct*Nup188 (Figure S5B). For this interaction, the C-terminal domain of *ct*Nup192 ($Nup192_{549–1756}$) was sufficient, although binding was reduced compared to the full-length protein. These data suggest that the folded Nup192 or Nup188 proteins, rather than a short sequence, interact with the helix motif of Nic96. Notably, conserved hydrophobic amino acids in the *ct*Nic96 helix are important for binding, as their mutation to alanines reduced binding to *ct*Nup192 (Figure S5C). Similarly, mutation of the orthologous conserved hydrophobic residues in the yeast Nic96 helix significantly diminished the two-hybrid interaction with yeast Nup192 or Nup188 (Figure S5C), suggesting that these mutations have a similar effect in yeast. Thus, a conserved helix motif in the Nic96 N domain mediates the formation of a complex with Nup192 or Nup188, possibly by binding to a hydrophobic patch on the solenoid surface of these large Nups.

To clarify whether Nic96, Nup192, and Nup188 can form a heterotrimer, ProtA-*ct*Nup188 immobilized on IgG beads was first incubated with 10-fold molar excess of *ct*Nup192, but no binding was observed (Figure 3C). Notably, when ProtA-*ct*Nup188 was incubated with both *ct*Nup192 and *ct*Nic96, binding of Nic96 to Nup188 was strongly decreased with recovery of both Nup192 and Nic96 in the unbound fraction (Figure 3C). Altogether these data indicate that stoichiometric Nup192-Nic96 and Nup188-Nic96 heterodimers but no tertiary complex can be formed in vitro. Apparently, Nup192 and Nup188 compete for the same binding site (i.e., the α helix motif) on Nic96.

Encouraged by the finding that interactions involving large *ct*Nups can be efficiently reconstituted in vitro, we extended our studies to other *ct*Nups. In particular, we focused on interactions between *ct*Nup53 (*C. thermophilum* has only one

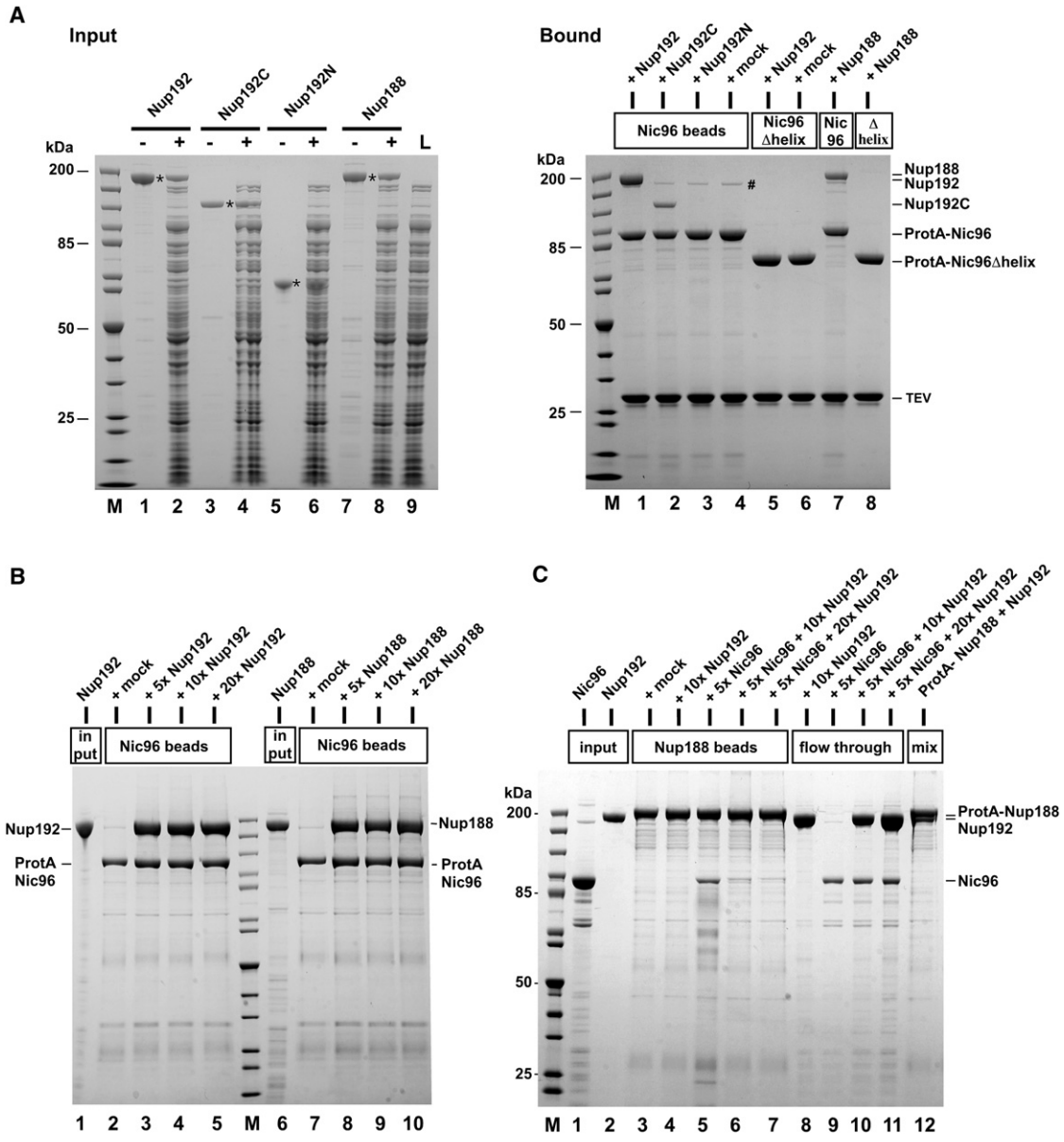

Figure 3. An α Helix Motif in the Nic96 N Domain Is Necessary and Sufficient for Binding to Nup192 or Nup188

(A) ProtA-TEV-*ct*Nic96 containing the α helix motif (for sequence see Figure S5A) or lacking it (*ct*Nic96Δhelix) was immobilized on IgG-Sepharose before addition of purified full-length *ct*Nup192, *ct*Nup188, *ct*Nup192C, or *ct*Nup192N mixed with an *E. coli* lysate (Input, +L). After binding and washing, it was eluted with TEV and the indicated eluates were analyzed by SDS-PAGE and Coomassie staining (Bound). The band (#) corresponds to endogenous yeast Nup192 coenriching with ProtA-*ct*Nic96 during affinity purification.

(B) Stoichiometric binding of *ct*Nic96 to either *ct*Nup192 or *ct*Nup188. Immobilized ProtA-TEV-*ct*Nic96 was incubated with increasing amounts of *ct*Nup192 or *ct*Nup188. It was eluted by acidic pH and the indicated eluates were analyzed by SDS-PAGE and Coomassie staining.

(C) ProtA-*ct*Nup188 immobilized on IgG-Sepharose was incubated with increasing amounts of *ct*Nup192 or *ct*Nic96, either separated or mixed. Input (lanes 1 and 2), bound material (eluted by acidic pH, lanes 3–7), and flowthrough fractions (lanes 8–11) were analyzed by SDS-PAGE and Coomassie staining. Mixing of ProtA-Nup188 and Nup192 revealed that SDS-PAGE can separate both bands (lane 12).

See also Figure S5.

Nup53/Nup59 ortholog) and *ct*Nup192, *ct*Nup170, and *ct*Nic96 (see Figures 1A and 1B). We performed in vitro binding assays, essentially as outlined above using the purified *ct*Nups present in a competitive lysate. Using this method, we were able to reconstitute heterodimeric complexes between (1) *ct*Nup53 and *ct*Nup192 (Figure 4A, lane 2), (2) *ct*Nup53 and *ct*Nic96 (lane 3), and (3) *ct*Nup53 and *ct*Nup170 (lane 4). *ct*Nup53 also interacted with *ct*Nup188 but less strongly than with *ct*Nup192 (Figure S6A).

To investigate which domains/motifs in Nup53 mediate these different interactions, we generated a series of Nup53 deletion

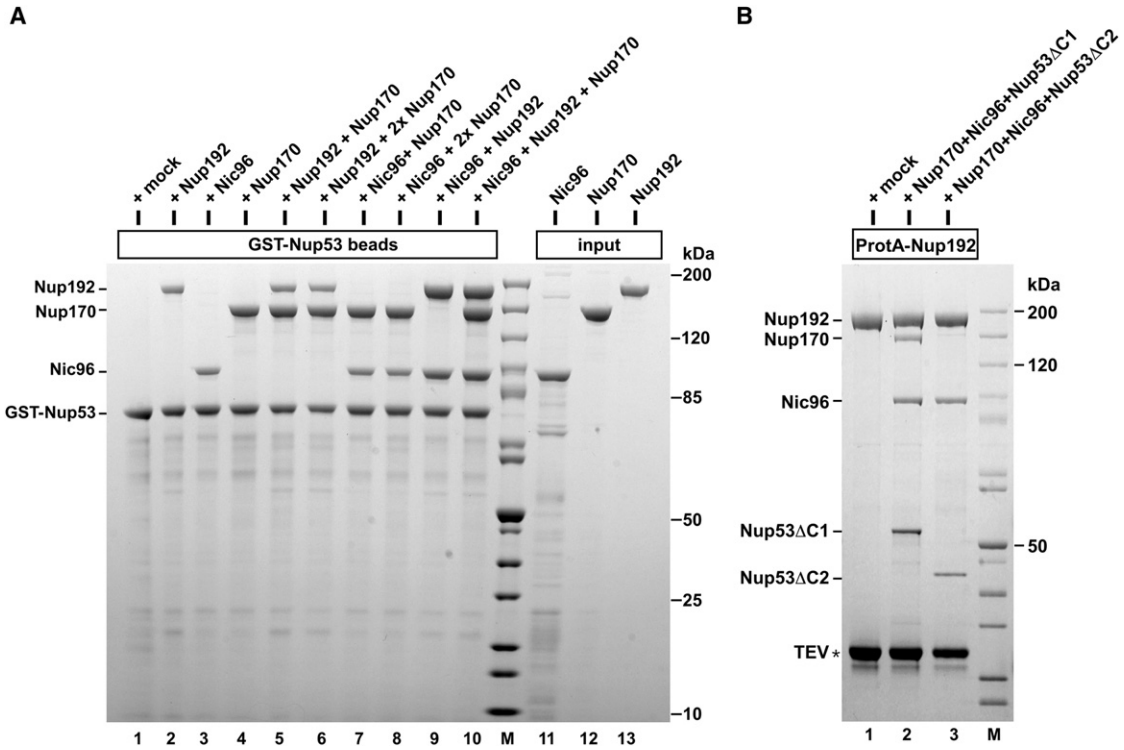

Figure 4. Reconstitution of the Tetrameric Nup192-Nup170-Nic96-Nup53 Complex with *C. thermophilum* Nucleoporins

(A) GST-*ct*Nup53 was immobilized on GSH beads before addition of purified *ct*Nic96, *ct*Nup170, and *ct*Nup192 (input, lanes 11–13), in the presence of competitive *E. coli* lysate. After binding and washing, it was eluted with SDS-sample buffer and eluates were analyzed by SDS-PAGE and Coomassie staining (lanes 1–10).

(B) Reconstitution of the *ct*Nup192-Nup170-Nic96-Nup53 module by using immobilized ProtA-*ct*Nup192 and addition of purified *ct*Nup170, *ct*Nic96, and *ct*Nup53ΔC1 or *ct*Nup53ΔC2 in the presence of an *E. coli* lysate. Bound material was eluted by TEV and analyzed by SDS-PAGE and Coomassie staining. See also Figure S6.

constructs. In addition to an amphipathic α helix at the C terminus that binds the pore membrane protein Ndc1 or can directly insert into membranes (Marelli et al., 2001; Onischenko et al., 2009), Nup53 contains a conserved RRM-like (RNA recognition motif) domain (Handa et al., 2006). Thus, *ct*Nup53 was divided into an N fragment (residues 1–88), RRM domain (133–252), C fragment (residues 329–389), and C-terminal amphipathic α helix (390–427) (Figures 5A and 5B). Following this domain classification, different *ct*Nup53 constructs were generated and tested for interaction with other Nups. *ct*Nic96 and *ct*Nup192 bound efficiently to the N fragment of *ct*Nup53 (Figure 5C, lanes 1–6), whereas *ct*Nup170 was recruited by the C fragment (Figure 5C, lanes 7–12, 15–16). In contrast, neither the RRM-like domain nor the C-terminal amphipathic α helix were required for these interactions in vitro. Further shortening of the N domain identified a sequence between residues 30 to 70, which was sufficient for binding to *ct*Nup192 or *ct*Nic96, albeit with reduced affinity (data not shown). Whether a Phe-Gly (FG) peptide present in the Nup53 N domain (Figure 5B) is directly involved in binding to Nup192 or Nic96 awaits further structural analysis.

Finally, we investigated whether the C-terminal domain of *ct*Nic96 (*ct*Nic96Δhelix) and *ct*Nup192 can simultaneously bind to the N fragment of *ct*Nup53 or whether these interactions are mutually exclusive. *ct*Nic96Δhelix was still capable of interacting with the Nup53-N motif (we used the larger Nup53-N+RRM construct that can be better determined on the SDS-polyacrylamide gel), whereas interaction with *ct*Nup192 was abolished (Figure S5D; see also Figure 3A). Similarly, when *ct*Nic96Δhelix was incubated with both *ct*Nup53-N+RRM and *ct*Nup192, only Nup53 but no Nup192 was coenriched (Figure S5D). Because Nup192 per se is competent to interact with the Nup53-N motif (see Figure 5C), these data suggest that Nup192 and Nic96 compete for the same binding site within the Nup53 N domain.

In Vitro Assembly of the Inner Nuclear Pore Ring Complex

In light of our observation that *ct*Nic96 and *ct*Nup53 have short motifs involved in multiple contacts to the large structural Nups, we extended the binding studies and tested whether more complicated assemblies can be reconstituted between the various structural *ct*Nups. In order to do this, we immobilized GST-*ct*Nup53 on beads and sequentially added the respective purified *ct*Nups. In this way, it was possible to reconstitute heterotrimeric complexes between *ct*Nup192, *ct*Nup170, and GST-*ct*Nup53 (Figure 4A, lane 5); *ct*Nic96, *ct*Nup170, and GST-*ct*Nup53 (Figure 4A, lane 7); and *ct*Nup192, *ct*Nic96, and GST-*ct*Nup53 (Figure 4A, lane 9). Both the Nup192-Nup170-Nup53

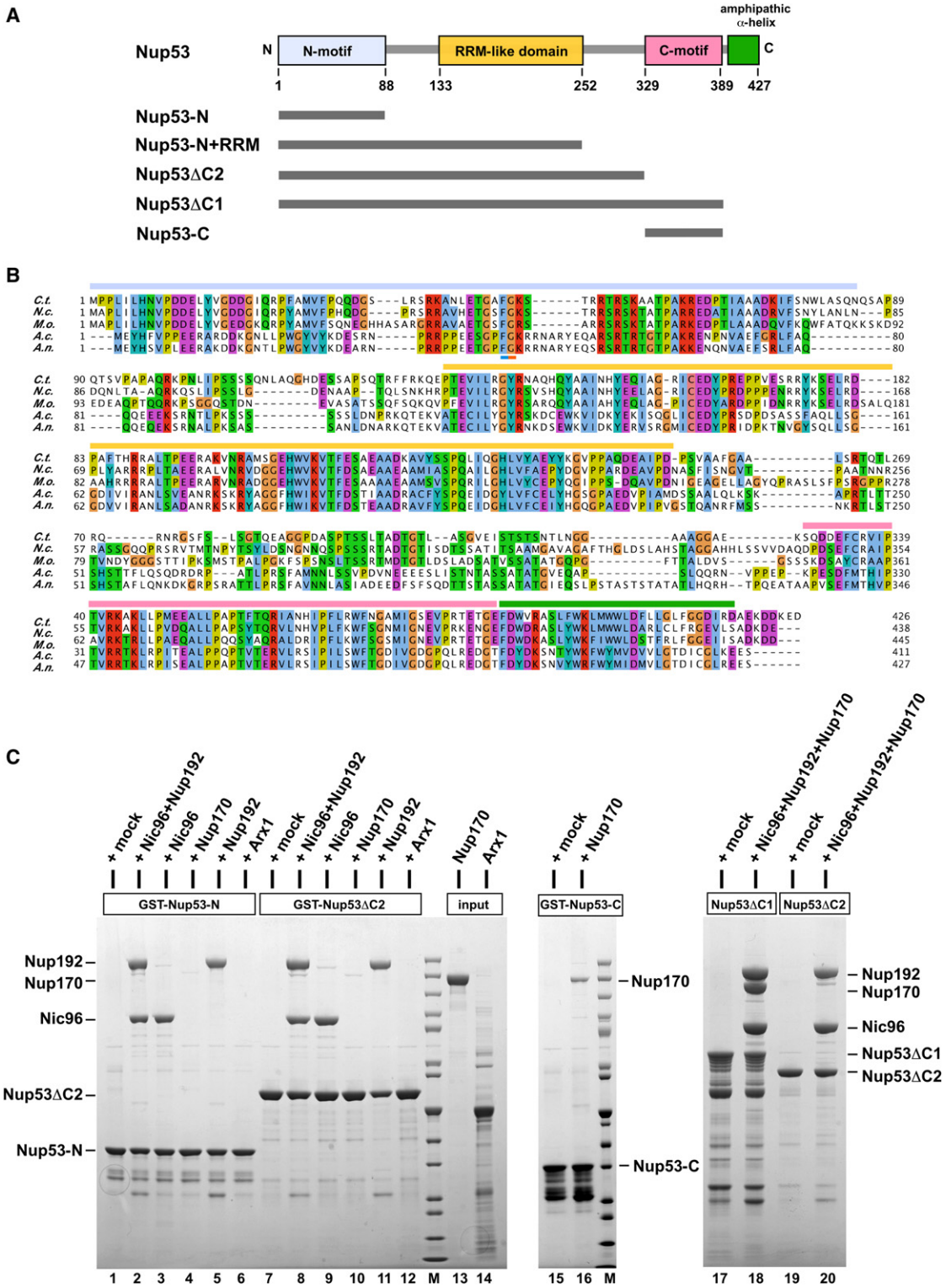

Figure 5. Nup53 Is a Multivalent Binding Protein Interacting with Nup192, Nic96, and Nup170

(A) Domain organization of *ct*Nup53. Below the schematic drawing are *ct*Nup53 deletion constructs used for the in vitro binding studies.

(B) Amino acid sequence alignment of Nup53 orthologs from *Chaetomium thermophilum* (*C.t.*), *Neurospora crassa* (*N.c.*), *Magnaporthe oryzae* (*M.o.*), *Aspergillus clavatus* (*A.c.*), and *Aspergillus niger* (*A.n.*).

and Nic96-Nup170-Nup53 complexes were efficiently formed even in the presence of excess *ct*Nup170. This is consistent with the observation that *ct*Nup170 binds to the C domain, whereas *ct*Nup192 or *ct*Nic96 bind to the N domain of *ct*Nup53 (see above). Finally, a heterotetrameric complex between *ct*Nup192, *ct*Nup170, *ct*Nic96, and GST-*ct*Nup53, in which all subunits were present in stoichiometric amounts due to the cooperative binding of *ct*Nup192 and *ct*Nic96, could be efficiently reconstituted (Figure 4A, lane 10). Similarly, this heterotetrameric complex could be formed in a different way by first immobilizing ProtA-Nup192 on IgG-Sepharose followed by reciprocal addition of the other purified components (Figure 4B). Recruitment of *ct*Nup170 to this module was solely dependent on the C motif in Nup53. This was apparent because a *ct*Nup53 construct lacking this motif (*ct*Nup53ΔC2) was associated with the absence of *ct*Nup170 from the module, whereas a *ct*Nup53 construct carrying this motif (*ct*Nup53ΔC1) was associated with inclusion of *ct*Nup170 in the module (Figure 5C, lanes 17–20 and Figure 4B).

Finally, a related tetrameric complex could be assembled in which *ct*Nup192 was replaced by *ct*Nup188. However, this tetramer contained slightly reduced amounts of *ct*Nup188 (Figures S6B and S6C), which is explained by the observation that *ct*Nup53 has lower affinity to *ct*Nup188 than to *ct*Nup192 (see Figure S6A). In conclusion, we have reconstituted an NPC module composed of the large solenoid Nup192 (or Nup188) together with Nup170, Nic96, and Nup53 and defined the motifs/domains by which these four Nups interact. Most of the Nups that are part of this module are implicated in formation of the inner nuclear pore ring (see Discussion).

Structural Insight into the Components of the Inner Pore Ring Module

To gain structural insight into the components of the inner pore ring, we used electron microscopy (EM) to analyze the structure of *ct*Nup192, *ct*Nup188, and *ct*Nup170. Overview pictures of the negatively stained proteins revealed a homogeneous distribution of particles. Accordingly, *ct*Nup170 exhibits a crescent-shaped structure with one bulbous end (15 nm length, 6 nm width), which is similar to yeast Nup170 (Figure 6A, see Flemming et al., 2009).

Markedly, the EM structures of *ct*Nup192 and *ct*Nup188 significantly differ from *ct*Nup170. Although not similar in their primary sequence, *ct*Nup192 and *ct*Nup188 exhibit comparable S-like structures (18 nm length, 10 nm width) with the two semicircles twisted by approximately 90° (Figure 6B, Figure S7A). Labeling of *ct*Nup192 with a prominent EM label (DID-Dyn2) (Flemming et al., 2010) revealed that the N and C termini are located at the respective tips of the S-shaped molecule (Figure 6C). When comparing the unusual S-like morphology of the α-helically predicted Nup192 molecule to known structures, we noticed that each of the two half circles of Nup192 resembles, in both shape and curvature, the karyopherin transport receptors (e.g., exportin-t or Crm1) that share a superhelical architecture of tandem HEAT repeats (Figure 6D, Movie S1).

Moreover, to mark the contact site of Nic96 on the surface of the S-shaped Nup192 molecule, the structural DID-Dyn2 label was first attached to the *ct*Nic96 helix followed by incubation with purified *ct*Nup192. Biochemical analysis indicated an efficient binding of the labeled Nic96 helix to Nup192, and EM revealed that the attached structural label stuck out from the S-shaped Nup192 molecule (Figure S7B). These data are consistent with the two-hybrid and biochemical data, which indicated that the Nic96 helix binds optimally to full-length Nup192, but that reduced binding to the C domain ($Nup192_{549–1756}$) was still possible.

We also investigated the trimeric Nup192-Nic96-Nup53 and tetrameric Nup192-Nup170-Nic96-Nup53 complexes by negative-stain EM and selected in both cases approximately 10,000 single particles of each for image analysis. In the case of the trimer, class averages were obtained revealing the typical S-shaped Nup192 molecule but with a diagonally overlaid elongated structure. This density could correspond to Nic96, known to be an ~8 nm long rod-like molecule (Figure S7C) (see Schrader et al., 2008). Nup53 consists of a globular RRM domain, approximately 3 nm in size (Handa et al., 2006), with attached short and flexible N and C domains. However, the precise position of Nup53 in this EM structure is unclear. In the case of the negatively stained tetrameric complex, a larger variety of class averages was obtained, which we attribute to structural variability of the inner pore ring module due to a more flexible attachment of Nup170 to the Nup192-Nic96-Nup53 core complex (data not shown).

In conclusion, EM analysis revealed the morphology of the Nups constituting the inner pore ring module and uncovered an unexpected structural similarity of α-helically predicted Nup192 and Nup188 to karyopherins. This latter observation supports speculation about the evolution of Nups and shuttling transport receptors that are members of the karyopherin superfamily (see Discussion).

DISCUSSION

In this study, we exploit a thermophilic eukaryote for biochemical and structural investigations of large nucleoporins that have previously proven to be difficult to handle when derived from several mesophilic organisms including yeast and humans. Due to the superior biophysical and biochemical properties of *C. thermophilum* proteins, we were able to reconstitute and assemble a conserved module of the nuclear pore complex. This study raises the possibility that this thermophile could serve as a model organism for numerous other eukaryotic complexes that, to date, have been difficult to handle biochemically. By providing a public genome and proteome of a thermophilic

(C) Distinct motifs in *ct*Nup53 bind *ct*Nup192, *ct*Nic96, and *ct*Nup170. Binding studies were performed on GSH beads with immobilized full-length GST-*ct*Nup53 and the indicated deletion constructs to which the indicated purified proteins in the presence of *E. coli* lysate were added. *ct*Arx1 (50 kDa) served as negative control.
See also Figure S5D.

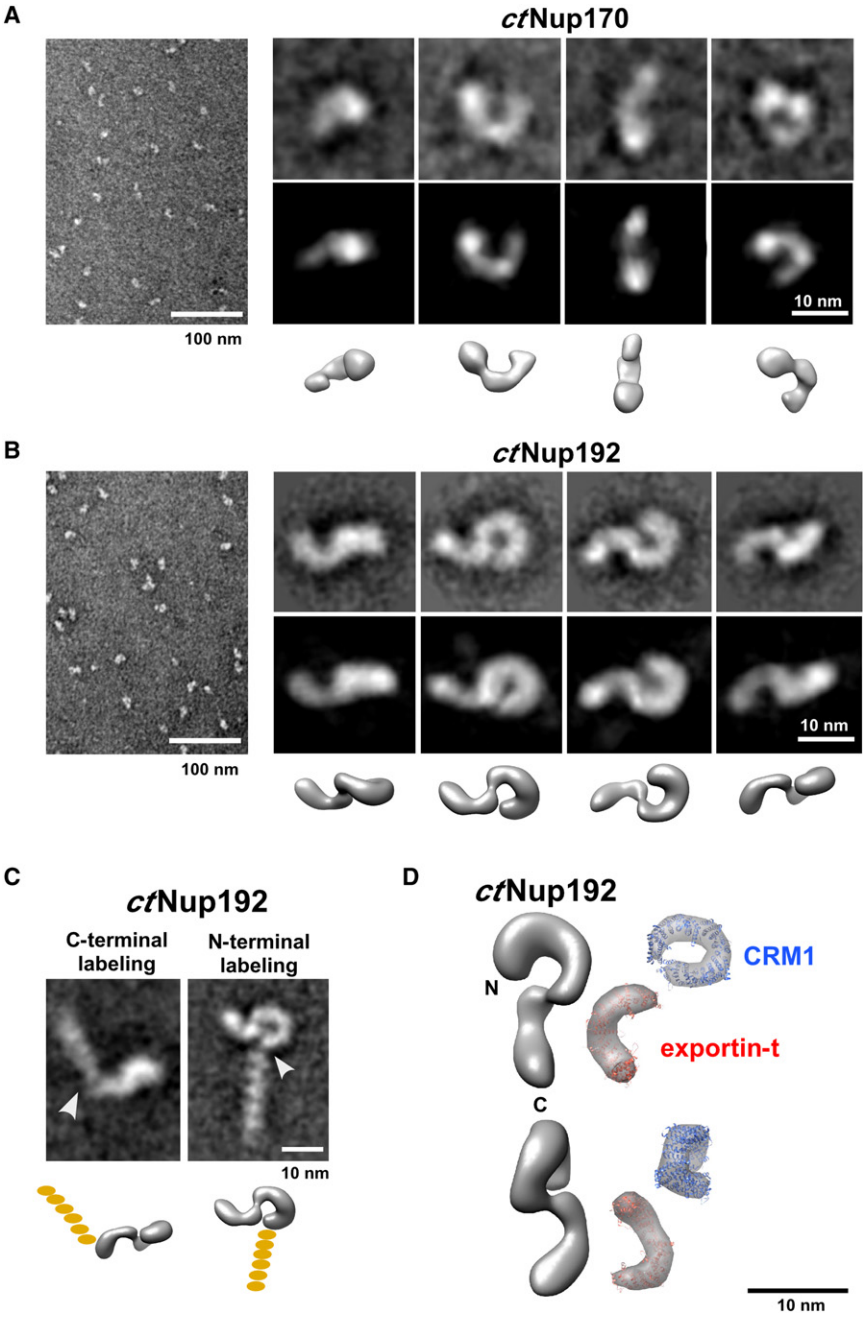

Figure 6. EM Analysis of *ct*Nup170 and *ct*Nup192

(A and B) Electron micrographs of purified *ct*Nup170 (A) and *ct*Nup192 (B). Overviews (left) and class averages (top row) of particles determined by multivariate statistical analysis agree with reprojections of the final 3D model (middle) and surface representations of the equivalent orientations (bottom).

(C) Labeling of *ct*Nup192 at the C terminus (left) and N terminus (right) with the DID-Dyn2 label. The arrow indicates the emergence of the label from the *ct*Nup192 molecule.

(D) Three-dimensional reconstruction of *ct*Nup192 with indicated N and C termini (left) compared to the atomic structures and calculated density maps (30 Å resolution) of exportin-t (red, PDB: 3IBV) and CRM1 (blue, PDB: 3GB8).

See also Figure S7, Movie S1, and Table S3.

eukaryote, we hope to have created a rich resource for structural biology and biotechnology, which should be valuable for a broad range of applications including structural proteomics and biotechnological developments.

Annotation of the ensemble of NPC proteins from *C. thermophilum* indicated that all of the known conserved Nups from various mesophilic organisms are present in this thermophile (Table S2, Figure S3, and Figure S4). In some respects, the *C. thermophilum* nucleoporins resemble those of vertebrates better than the model organism yeast does. For example, in contrast to yeast, we identified orthologs of Nup37 *and* Elys in the *C. thermophilum* genome, as has been shown for *A. nidulans,* which is also a member of the *Pezizomycotina* clade. Therefore, the corresponding *ct*Nup84 complex appears to be more related to the vertebrate Nup107-Nup160 complex than to the yeast Nup84 complex (D'Angelo and Hetzer, 2008). On the other hand, *C. thermophilum* is closely related to *N. crassa* and *A. nidulans* (see above), which both exhibit a closed mitosis with no breakdown of the nuclear envelope. Thus, we predict that the thermophile also divides by closed mitosis. However, it remains unknown whether the NPC partially disassembles during mitosis as observed for *A. nidulans* (De Souza et al., 2004), or whether it stays intact as described for *N. crassa* (Roca et al., 2010). Development of a transformation system combined with homologous integration of a GFP reporter at different *ctNUP* loci could enable us to differentiate between these possibilities.

C. thermophilum also contains orthologs of the nuclear pore membrane spanning Nups including Ndc1, Pom152, and Pom34, which may be linked to the structural Nups of the inner pore ring (i.e., Nup170, Nup53; see below). In the case of the Nups that constitute the nuclear basket, we have identified a clear *C. thermophilum* ortholog of Mlp1 (Tpr1 in higher eukaryotes); however, Nup1 (Nup153 in vertebrates), Nup2, and Nup60 could not be identified based on homology searches. In general, the Nups forming the nuclear basket are poorly conserved in evolution, making it difficult to assign corresponding orthologs. However, two putative *ct*Nups, *ct*Nup56 and *ct*Nup152, which contain FG repeats and predicted Ran-binding domains (Table S2 and Figure S3), are candidates for nuclear basket proteins.

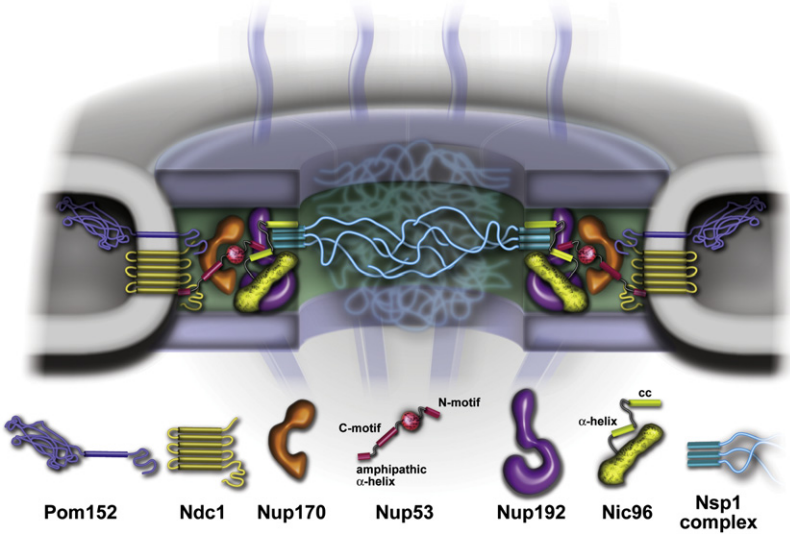

Figure 7. Model of the Inner Pore Ring Complex in the NPC

Schematic drawing of the NPC in the nuclear envelope. The inner pore ring (green) is composed of Nup192 and Nup170, bridged by short and flexible motifs provided by linker Nups, Nup53 and Nic96. Nup53 is connected to the pore membrane protein Ndc1 and Nup170 to Pom152. Nic96 binds via the helix motif to Nup192 and via the coiled-coil domain (cc) to the Nsp1 complex, from which FG repeat filaments protrude into the central pore channel.

Our studies revealed that the large *ct*Nups have excellent biochemical and structural properties, allowing the reconstitution of one of the long sought-after key modules of the NPC, the inner pore ring complex. This achievement was possible because two-hybrid and genetic analyses in yeast could be combined with in vitro assembly of the orthologous Nups from the thermophile. The reconstituted NPC module has the potential to span the entire width of the NPC, from the anchoring membrane to the central FG repeat-containing transport channel (Figure 7). This conclusion is supported by several findings. First, one subunit of the module, Nup53, can directly bind via its C-terminal amphipathic α helix to the pore membrane involving the integral membrane protein Ndc1 (Onischenko et al., 2009). Second, Nup170 in yeast is functionally linked to another pore membrane protein Pom152 (Marelli et al., 2001; Tcheperegine et al., 1999), suggesting that a Nup170-Pom152 interaction further contributes to pore membrane anchorage of the inner pore ring module. Third, another subunit, Nic96, can recruit the Nsp1-Nup49-Nup57 complex that is part of the central FG transport channel. Fourth, the estimated size of the Nup192-Nup170-Nic96-Nup53 tetramer (approximately 20–25 nm) is consistent with such a complete bridging, taking into account the known dimensions of the central FG transport channel (approximately 38 nm) and the overall NPC diameter (approximately 98 nm) (Alber et al., 2007).

This investigation provided insight into the mechanism of how the large structural proteins Nup192, Nup188, and Nup170/Nup157 interact with Nic96 and Nup53. In the past, hints as to how these Nups could be organized in subcomplexes came from studies not only in yeast (see Introduction) but also in higher eukaryotes, which revealed that vertebrate Nup53 can interact with a number of Nups including Nup93 (yNic96), Nup155 (yNup170), Nup205 (yNup192), and Ndc1 (Hawryluk-Gara et al., 2005). However, it remained unclear whether Nup205, Nup188, and Nup93 are part of a subcomplex (Miller et al., 2000) or are assembled in separate modules (Theerthagiri et al., 2010). Our studies have demonstrated that heterodimeric complexes, Nup192-Nic96 and Nup188-Nic96, can be assembled, but a supercomplex between Nup192, Nup188, and Nic96 is not formed. Thus, binding of the Nic96 α helix motif to the two large solenoid Nups is mutually exclusive. This finding supports the data from the Antonin lab, which revealed that vertebrate Nup93 is part of two distinct subcomplexes, interacting either with Nup205 or Nup188 (Theerthagiri et al., 2010).

Moreover, we discovered that the large structural Nups of the inner pore ring do not directly interact but are flexibly bridged by short linear motifs provided by linker Nups. This indicates a previously unrecognized mode of Nup interaction within the NPC. Previously described Nup-Nup contacts involve coiled-coil interactions (e.g., within the Nsp1/p62 complex) and interactions between folded α-helical domains (e.g., between Nup84 and Nup145C; Nagy et al., 2009) or between folded α-helical and β-propeller domains (e.g., between Sec13 and Nup145; Brohawn and Schwartz, 2009). Here, we found that in the case of Nic96, the interacting motif is a conserved predicted α helix protruding from the flexible Nic96 N domain and docking onto the solenoid surface of either Nup192 or Nup188, an interaction that appears to be mutually exclusive. Similarly, in the case of Nup53, short linear motifs present in the flexible N and C domains make direct contact with all three inner pore ring Nups, Nup192, Nic96, and Nup170, thereby stabilizing the entire module by multiple "crosslinks." Such a mode of interaction could allow for structural flexibility and variability within the inner pore ring module that directly adjoins to a layer of Nups that line the central transport channel (Figure 7). In this way, the central transport channel could dilate or shrink depending on the size of the passing transport cargo.

The excellent biophysical properties of the *ct*Nups also facilitated single particle EM analysis, which gave insight into the structural organization of the large solenoid Nups. When comparing the unusual S-like morphology of the α-helically predicted Nup192 molecule to known structures, we noticed that each of the two half circles of Nup192 resembles, in both shape and curvature, karyopherin transport receptors (e.g., exportin-t or Crm1) (Figure 6D and Movie S1). Very little is known about the fold type of the two largest Nups, Nup188 and Nup192/Nup205, in any eukaryote, except that they are mainly α helical and adopt a SPAH (stacked *p*airs of α-*h*elices) fold (Devos et al., 2006). Indeed, bioinformatic analysis indicates that

Nup192 and Nup188 are similar to karyopherins (e.g., Crm1, exportin-t) in terms of tertiary structure (Table S3). Accordingly, it is possible that Nups and karyopherins share a common evolutionary origin (Devos et al., 2006). One plausible scenario could be that an ancestral Nup (Nup192-like) may have lost its ability to stably assemble into the NPC, e.g., by altering a binding groove for a linear "Nup motif" on its solenoid surface so that a "NES motif" could be adopted. Thus, the binding mode of a SPAH Nup to a linear motif of a linker Nup could be similar to the mechanism of how karyopherins interact with cargo.

In conclusion, our analyses using nucleoporins from a thermophile identified a central complex of the NPC and offer support to the possibility of an evolutionary relationship between the gate and the transporters, the NPC and the karyopherins.

EXPERIMENTAL PROCEDURES

A detailed description of the methods employed in this study is provided in the Extended Experimental Procedures.

Strains, Media, and Plasmids

Plasmids generated by standard procedures are listed in Table S4. *Saccharomyces cerevisiae* strains used in this study are listed in Table S5.

Cloning of Nup Genes from *C. thermophilum*

C. thermophilum La Touche var. thermophilum was obtained from DSMZ, Braunschweig, Germany. Genomic DNA and total RNA were isolated according to standard procedures. cDNA was synthesized using Superscript-III Reverse Transcriptase (Invitrogen) and an Oligo d(T) primer according to the company's instructions. cDNA was purified with the QIAquick PCR purification Kit (QIAGEN). *C. thermophilum* Nup-encoding genes were cloned from either cDNA or genomic DNA using standard procedures. The *ct*Nup ORFs were inserted into yeast or *E. coli* expression plasmids.

Genome Sequencing and Analysis

DNA extraction was performed as previously described (Al-Samarrai and Schmid, 2000). The genome was sequenced using 454 GS FLX and 454 GS XLR technologies (Margulies et al., 2005; Ronaghi et al., 1996). These were assembled using Celera assembler (Miller et al., 2008) v5.3 resulting in 20 scaffolds with 24× coverage. Gene prediction was done by AUGUSTUS (Stanke and Waack, 2003) and manually for the mitochondrial genome. Protein-coding genes were annotated with SMART domains (Letunic et al., 2009).

Two-Hybrid Analysis

For yeast two-hybrid analysis, the yeast reporter strain PJ69-4A was cotransformed with the yeast Nup constructs fused to the *GAL4*-binding domain or *GAL4* activation domain (James et al., 1996).

Affinity Purification and In Vitro Binding Assays

Affinity purification of *ct*Nups using ProtA, GSH, or FLAG tags was performed on IgG-Sepharose, GSH beads, or FLAG-antibody beads.

Thermosolubility Test of Yeast and *C. thermophilum* Nups

To test for thermostability, yeast Nup170 and Nup192 and *ct*Nup192, *ct*Nup188, and *ct*Nup170, expressed in yeast under the control of the constitutive ADHI promoter, were affinity-purified via the ProtA-tag and incubated for 1 hr at different temperatures.

Electron Microscopy and Image Processing

Negative stain EM using 2% (w/v) uranyl acetate and image processing were performed as described (Flemming et al., 2010). Spatial orientations of class averages were calculated by sinogramm correlation and combined to a three-dimensional (3D) map using the weighted back-projection algorithm.

Labeling of ProtA-*ct*Nup192 or ProtA-*ct*Nic96 helix with the structural Dyn2-DID marker was performed according to Flemming et al. (2010).

ACCESSION NUMBERS

The nuclear genome sequences of *Chaetomium thermophilum var. thermophilum* DSM 1495 reported in this paper have been deposited at DDBJ/EMBL/GenBank under the accession number ADUW00000000. The version described in this paper is the first version, ADUW01000000. The complete mitochondrial genome has been deposited at DDBJ/EMBL/GenBank under the accession number JN007486. Moreover, the DNA and protein sequences of the *ct*Nups described in this study have been deposited at NCBI with the accession numbers indicated in Table S2.

SUPPLEMENTAL INFORMATION

Supplemental Information includes Extended Experimental Procedures, seven figures, five tables, and one movie and can be found with this article online at doi:10.1016/j.cell.2011.06.039.

ACKNOWLEDGMENTS

We thank Eurofins MWG Operon, in particular Dr. Georg Gradl, for a very competent cooperation in the DNA sequencing project. We thank Christian von Mering for help using the eggNOG pipeline and Sheila Lutz for initial help in setting up blast searches using the *C. thermophilum* genomic sequence. We thank Andrea Hellwig (Prof. Hilmar Bading, Department of Neurobiology, University of Heidelberg) for performing thin-section electron microscopy. E.H. is recipient of grants from the Deutsche Forschungsgemeinschaft (SFB 638/B2).

Received: November 30, 2010
Revised: April 15, 2011
Accepted: June 24, 2011
Published: July 21, 2011

REFERENCES

Al-Samarrai, T.H., and Schmid, J. (2000). A simple method for extraction of fungal genomic DNA. Lett. Appl. Microbiol. *30*, 53–56.

Alber, F., Dokudovskaya, S., Veenhoff, L.M., Zhang, W., Kipper, J., Devos, D., Suprapto, A., Karni-Schmidt, O., Williams, R., Chait, B.T., et al. (2007). The molecular architecture of the nuclear pore complex. Nature *450*, 695–701.

Altschul, S.F., Madden, T.L., Schäffer, A.A., Zhang, J., Zhang, Z., Miller, W., and Lipman, D.J. (1997). Gapped BLAST and PSI-BLAST: a new generation of protein database search programs. Nucleic Acids Res. *25*, 3389–3402.

Belgareh, N., Snay-Hodge, C., Pasteau, F., Dagher, S., Cole, C.N., and Doye, V. (1998). Functional characterization of a Nup159p-containing nuclear pore subcomplex. Mol. Biol. Cell *9*, 3475–3492.

Brohawn, S.G., Leksa, N.C., Spear, E.D., Rajashankar, K.R., and Schwartz, T.U. (2008). Structural evidence for common ancestry of the nuclear pore complex and vesicle coats. Science *322*, 1369–1373.

Brohawn, S.G., and Schwartz, T.U. (2009). Molecular architecture of the Nup84-Nup145C-Sec13 edge element in the nuclear pore complex lattice. Nat. Struct. Mol. Biol. *16*, 1173–1177.

Cronshaw, J.M., Krutchinsky, A.N., Zhang, W., Chait, B.T., and Matunis, M.J. (2002). Proteomic analysis of the mammalian nuclear pore complex. J. Cell Biol. *158*, 915–927.

D'Angelo, M.A., and Hetzer, M.W. (2008). Structure, dynamics and function of nuclear pore complexes. Trends Cell Biol. *18*, 456–466.

De Souza, C.P., Osmani, A.H., Hashmi, S.B., and Osmani, S.A. (2004). Partial nuclear pore complex disassembly during closed mitosis in *Aspergillus nidulans*. Curr. Biol. *14*, 1973–1984.

Devos, D., Dokudovskaya, S., Alber, F., Williams, R., Chait, B.T., Sali, A., and Rout, M.P. (2004). Components of coated vesicles and nuclear pore complexes share a common molecular architecture. PLoS Biol. *2*, e380.

Devos, D., Dokudovskaya, S., Williams, R., Alber, F., Eswar, N., Chait, B.T., Rout, M.P., and Sali, A. (2006). Simple fold composition and modular architecture of the nuclear pore complex. Proc. Natl. Acad. Sci. USA *103*, 2172–2177.

Dilworth, D.J., Suprapto, A., Padovan, J.C., Chait, B.T., Wozniak, R.W., Rout, M.P., and Aitchison, J.D. (2001). Nup2p dynamically associates with the distal regions of the yeast nuclear pore complex. J. Cell Biol. *153*, 1465–1478.

Doye, V., and Hurt, E. (1997). From nucleoporins to nuclear pore complexes. Curr. Opin. Cell Biol. *9*, 401–411.

Fahrenkrog, B., and Aebi, U. (2003). The nuclear pore complex: nucleocytoplasmic transport and beyond. Nat. Rev. Mol. Cell Biol. *4*, 757–766.

Fahrenkrog, B., Hübner, W., Mandinova, A., Panté, N., Keller, W., and Aebi, U. (2000). The yeast nucleoporin Nup53p specifically interacts with Nic96p and is directly involved in nuclear protein import. Mol. Biol. Cell *11*, 3885–3896.

Flemming, D., Sarges, P., Stelter, P., Hellwig, A., Böttcher, B., and Hurt, E. (2009). Two structurally distinct domains of the nucleoporin Nup170 cooperate to tether a subset of nucleoporins to nuclear pores. J. Cell Biol. *185*, 387–395.

Flemming, D., Thierbach, K., Stelter, P., Böttcher, B., and Hurt, E. (2010). Precise mapping of subunits in multiprotein complexes by a versatile electron microscopy label. Nat. Struct. Mol. Biol. *17*, 775–778.

Grandi, P., Doye, V., and Hurt, E.C. (1993). Purification of NSP1 reveals complex formation with 'GLFG' nucleoporins and a novel nuclear pore protein NIC96. EMBO J. *12*, 3061–3071.

Hakulinen, N., Turunen, O., Jänis, J., Leisola, M., and Rouvinen, J. (2003). Three-dimensional structures of thermophilic beta-1,4-xylanases from Chaetomium thermophilum and Nonomuraea flexuosa. Comparison of twelve xylanases in relation to their thermal stability. Eur. J. Biochem. *270*, 1399–1412.

Handa, N., Kukimoto-Niino, M., Akasaka, R., Kishishita, S., Murayama, K., Terada, T., Inoue, M., Kigawa, T., Kose, S., Imamoto, N., et al. (2006). The crystal structure of mouse Nup35 reveals atypical RNP motifs and novel homodimerization of the RRM domain. J. Mol. Biol. *363*, 114–124.

Hawryluk-Gara, L.A., Shibuya, E.K., and Wozniak, R.W. (2005). Vertebrate Nup53 interacts with the nuclear lamina and is required for the assembly of a Nup93-containing complex. Mol. Biol. Cell *16*, 2382–2394.

Hickey, D.A., and Singer, G.A. (2004). Genomic and proteomic adaptations to growth at high temperature. Genome Biol. *5*, 117.

Hsia, K.C., Stavropoulos, P., Blobel, G., and Hoelz, A. (2007). Architecture of a coat for the nuclear pore membrane. Cell *131*, 1313–1326.

Hurwitz, M.E., Strambio-de-Castillia, C., and Blobel, G. (1998). Two yeast nuclear pore complex proteins involved in mRNA export form a cytoplasmically oriented subcomplex. Proc. Natl. Acad. Sci. USA *95*, 11241–11245.

James, P., Halladay, J., and Craig, E.A. (1996). Genomic libraries and a host strain designed for highly efficient two-hybrid selection in yeast. Genetics *144*, 1425–1436.

Kosova, B., Panté, N., Rollenhagen, C., and Hurt, E. (1999). Nup192p is a conserved nucleoporin with a preferential location at the inner site of the nuclear membrane. J. Biol. Chem. *274*, 22646–22651.

La Touche, C.J. (1948). A Chaetomium-like thermophile fungus. Nature *161*, 320.

Letunic, I., Doerks, T., and Bork, P. (2009). SMART 6: recent updates and new developments. Nucleic Acids Res. *37*(Database issue), D229–D232.

Makio, T., Stanton, L.H., Lin, C.C., Goldfarb, D.S., Weis, K., and Wozniak, R.W. (2009). The nucleoporins Nup170p and Nup157p are essential for nuclear pore complex assembly. J. Cell Biol. *185*, 459–473.

Marelli, M., Aitchison, J.D., and Wozniak, R.W. (1998). Specific binding of the karyopherin Kap121p to a subunit of the nuclear pore complex containing Nup53p, Nup59p, and Nup170p. J. Cell Biol. *143*, 1813–1830.

Marelli, M., Lusk, C.P., Chan, H., Aitchison, J.D., and Wozniak, R.W. (2001). A link between the synthesis of nucleoporins and the biogenesis of the nuclear envelope. J. Cell Biol. *153*, 709–724.

Margulies, M., Egholm, M., Altman, W.E., Attiya, S., Bader, J.S., Bemben, L.A., Berka, J., Braverman, M.S., Chen, Y.J., Chen, Z., et al. (2005). Genome sequencing in microfabricated high-density picolitre reactors. Nature *437*, 376–380.

Miller, B.R., Powers, M., Park, M., Fischer, W., and Forbes, D.J. (2000). Identification of a new vertebrate nucleoporin, Nup188, with the use of a novel organelle trap assay. Mol. Biol. Cell *11*, 3381–3396.

Miller, J.R., Delcher, A.L., Koren, S., Venter, E., Walenz, B.P., Brownley, A., Johnson, J., Li, K., Mobarry, C., and Sutton, G. (2008). Aggressive assembly of pyrosequencing reads with mates. Bioinformatics *24*, 2818–2824.

Muller, J., Szklarczyk, D., Julien, P., Letunic, I., Roth, A., Kuhn, M., Powell, S., von Mering, C., Doerks, T., Jensen, L.J., and Bork, P. (2010). eggNOG v2.0: extending the evolutionary genealogy of genes with enhanced non-supervised orthologous groups, species and functional annotations. Nucleic Acids Res. *38*(Database issue), D190–D195.

Nagy, V., Hsia, K.C., Debler, E.W., Kampmann, M., Davenport, A.M., Blobel, G., and Hoelz, A. (2009). Structure of a trimeric nucleoporin complex reveals alternate oligomerization states. Proc. Natl. Acad. Sci. USA *106*, 17693–17698.

Nehrbass, U., Rout, M.P., Maguire, S., Blobel, G., and Wozniak, R.W. (1996). The yeast nucleoporin Nup188p interacts genetically and physically with the core structures of the nuclear pore complex. J. Cell Biol. *133*, 1153–1162.

Onischenko, E., Stanton, L.H., Madrid, A.S., Kieselbach, T., and Weis, K. (2009). Role of the Ndc1 interaction network in yeast nuclear pore complex assembly and maintenance. J. Cell Biol. *185*, 475–491.

Patel, S.S., Belmont, B.J., Sante, J.M., and Rexach, M.F. (2007). Natively unfolded nucleoporins gate protein diffusion across the nuclear pore complex. Cell *129*, 83–96.

Roca, M.G., Kuo, H.C., Lichius, A., Freitag, M., and Read, N.D. (2010). Nuclear dynamics, mitosis, and the cytoskeleton during the early stages of colony initiation in Neurospora crassa. Eukaryot. Cell *9*, 1171–1183.

Ronaghi, M., Karamohamed, S., Pettersson, B., Uhlén, M., and Nyrén, P. (1996). Real-time DNA sequencing using detection of pyrophosphate release. Anal. Biochem. *242*, 84–89.

Rout, M.P., Aitchison, J.D., Suprapto, A., Hjertaas, K., Zhao, Y., and Chait, B.T. (2000). The yeast nuclear pore complex: composition, architecture, and transport mechanism. J. Cell Biol. *148*, 635–651.

Schrader, N., Stelter, P., Flemming, D., Kunze, R., Hurt, E., and Vetter, I.R. (2008). Structural basis of the nic96 subcomplex organization in the nuclear pore channel. Mol. Cell *29*, 46–55.

Siniossoglou, S., Wimmer, C., Rieger, M., Doye, V., Tekotte, H., Weise, C., Emig, S., Segref, A., and Hurt, E.C. (1996). A novel complex of nucleoporins, which includes Sec13p and a Sec13p homolog, is essential for normal nuclear pores. Cell *84*, 265–275.

Stanke, M., and Waack, S. (2003). Gene prediction with a hidden Markov model and a new intron submodel. Bioinformatics *19* (*Suppl 2*), ii215–ii225.

Tcheperegine, S.E., Marelli, M., and Wozniak, R.W. (1999). Topology and functional domains of the yeast pore membrane protein Pom152p. J. Biol. Chem. *274*, 5252–5258.

Theerthagiri, G., Eisenhardt, N., Schwarz, H., and Antonin, W. (2010). The nucleoporin Nup188 controls passage of membrane proteins across the nuclear pore complex. J. Cell Biol. *189*, 1129–1142.